NUCLEAR SCIENCE AND TECHNIQUES **26**, 060503 (2015)

FS23 binds to the N-terminal domain of human Hsp90: A novel small inhibitor for Hsp90*

LI Jian (李健),[1,2,†] SHI Feng (石峰),[3,†] CHEN Dan-Qi (陈丹琦),[3] CAO Hui-Ling (曹慧玲),[1] XIONG Bing (熊兵),[3] SHEN Jing-Kang (沈竞康),[3,‡] and HE Jian-Hua (何建华)[2,§]

[1] *Shanxi Key Laboratory of Ischemic Cardiovascular Disease; Institute of Basic & Translational Medicine, Xi'an Medical University, Xi'an 710021, China*
[2] *Shanghai Institute of Applied Physics, Chinese Academy of Sciences, Shanghai 201204, China*
[3] *Department of Medicinal Chemistry, State Key Laboratory of Drug Research, Shanghai Institute of Materia Medica, Chinese Academy of Sciences, Shanghai 201203, China*

(Received July 9, 2015; accepted in revised form July 25, 2015; published online December 20, 2015)

The N-terminal domain of heat shock protein 90 ($Hsp90^N$) is responsible for the catalytic activity of Hsp90. The reported inhibitors of Hsp90 bind to this domain and would inhibit tumor growth and progression. Here, we synthesized FS23, a small molecule inhibitor of hsp90 and collected X-ray diffraction data of the complex crystal of Hsp90-FS23. High resolution X-ray crystallography shows that FS23 interacted with $Hsp90^N$ at the nucleotide binding cleft, and this suggests that FS23 may complete with nucleotides to bind to $Hsp90^N$. The crystal structure and the interaction between $Hsp90^N$ and FS23 suggest a rational basis for the design of novel antitumor drugs.

Keywords: Heat shock protein 90, N-terminal domain, Inhibitor, X-ray diffraction, Interactions

DOI: 10.13538/j.1001-8042/nst.26.060503

I. INTRODUCTION

X-ray crystallography is now used routinely to determine how a pharmaceutical interacts with its protein target and what changes may improve it. It offers details of protein-ligand interactions and holds the promise for novel, more effective, safer and cheaper drugs. During the past decade, macromolecular crystallography has become a standard technique used by industries of pharmaceuticals and biotechnology [1, 2].

The heat shock protein 90 (Hsp90) is a homodimer, and each of its monomers consists of three domains: an N-terminal domain, a middle domain with a large hydrophobic surface to help folding its client proteins, and a C-terminal domain playing a prominent role in the constitutive dimerization [3–5]. The N-terminal domain ($Hsp90^N$) containing a highly conserved ATP binding site is essential for the function of Hsp90 [4]. The first X-ray structure of human $Hsp90^N$ by Stebbins *et al*. [6] reveals an α/β sandwich with a pronounced ligand-binding pocket, about 15 Å deep. On the 'floor' of this structure are eight uninterrupted antiparallel β sheets. The pocket walls are formed by three α helices and a loop. A helical face of the sandwich has a surface groove that leads into the pocket [6, 7].

Hsp90 has dual chaperone functions. One is participating in the conformational maturation and activation of a wide range of client proteins, many of which are known to play important roles in controlling proliferation, survival, invasion, metastasis and angiogenesis. The other is mediating the ATP-dependent refolding. These enlighten us that inhibitors of Hsp90 may cause potent inhibition of tumor growth and progression [8–10]. Hsp90 has attracted much interests as a therapeutic target for anticancer drugs since the findings that both geldanamycin (GDM) and radicicol could inhibit Hsp90 function by binding to an ATP binding pocket in the N-terminal domain of protein [5, 10–12].

As a naturally occurring antitumor antibiotic, GDM has been in preclinical development as an antitumor agent [5, 13, 14], but the mechanism was unknown until crystal structure of the complex of $Hsp90^N$-GDM was determined, suggesting that GDM acts by blocking the binding of ATP to Hsp90. Once the inhibitor binds to the pocket, the conformational/domain rearrangement of Hsp90 no longer takes place, leading to Hsp90 invalid in helping its client proteins to accomplish conformational maturation, stability and function [15–17]. Besides, naturally occurring antibiotics for Hsp90, such as radicicol and others, function in the similar ways. Unfortunately, this kind of antitumor antibiotics has side effects, such as their toxicity for liver, and studies have been conducted to find new ways for managing cancer through Hsp90α [18, 19]. Several derivatives of natural inhibitors like 17-AAG, 17-DMAG and IPI-504 have entered clinical studies [20–24]. However, there are several potential limitations, including poor solubility, limited bioavailability and hepatotoxicity with the compounds [21, 23]. These have led to significant efforts to identify small-molecule inhibitors.

Structure-based drug design (SBDD) has become a proven technique to find novel compounds as starting points for optimization. Compounds are selected by docking and tested in a biochemical assay. The confirmed hits are crystallized. Information from X-ray structures of the inhibitors are used to drive the drug evolution process [25–30].

To continue the efforts to discover new Hsp90 inhibitor,

* Supported by National Natural Science Foundation of China (No. 81402850), the Natural Science Basic Research Plan in Shaanxi Province of China (No. 2015JM3114), the Introduced talents Foundation of Xi'an Medical University (No. 2015 RCYJ01) and the Doctorate Foundation of Xi'an Medical University (No. 2015 DOC23)
† These authors contributed equally to this work.
‡ jkshen@simm.ac.cn
§ hejianhua@sinap.ac.cn

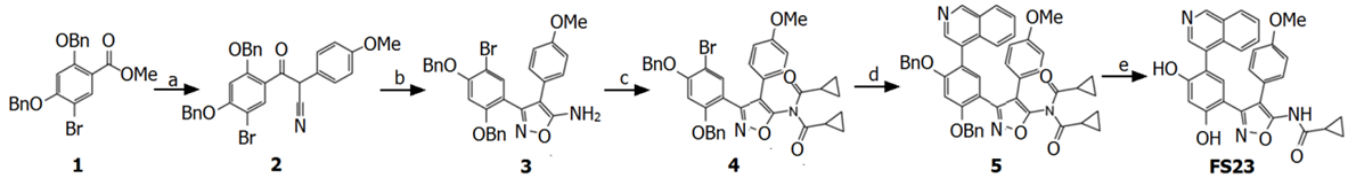

Fig. 1. Synthesis of the small molecule FS23. (a) 4-methoxy phenylacetonitrile, lithium hexamethyldisilazide, tetrahydrofuran, −78 °C, 1 h, 97.2%. (b) $NH_2OH \cdot HCl$, pyridine, 100 °C, 12 h, 54.7%. (c) Cyclopropanecarbonyl chloride, NEt_3, dichloromethane, 4-dimethylaminopyridine, 0 °C, 1 h, 90%. (d) Isoquinoline-4-boronic acid, $Pd(PPh_3)_4$, K_2CO_3, $CH_3OCH_2CH_2OCH_3/H_2O$, 120 °C, 1 h, 82.9%. (e) BCl_3, dichloromethane, rt, 1 h, 43.3%.

we synthesized a new inhibitor FS23, designed by merging bioactive fragments identified from fragment compounds (which are selected by docking and tested in a biochemical assay) screening and optimization with SBDD method. Subsequently, we resolved the crystal structure of $Hsp90^N$-FS23 complex by X-ray diffraction. The complex structure of $Hsp90^N$-FS23 provides the structural basis to further investigate the activated conformational change of Hsp90 after FS23 binding. The most interesting portion of the interface in the complex $Hsp90^N$-FS23 is the hole produced by structural rearrangements of L6. There is neither a direct nor an indirect interaction between residues in the hole and FS23. So groups could be added to FS23 to fill the cavity and interact with residues in the hole to increase the activity of derivatives.

II. EXPERIMENTAL

A. Synthesis of the small molecule FS23

As shown in Fig. 1, under reaction of lithium hexamethyldisilazide, Compound **1** was condensed with 4-methoxy phenylacetonitrile to give **2**, followed by cyclization with hydroxylamine hydrochloride to obtain Compound **3**, which reacted with cyclopropanecarbonyl chloride, and subsequently Suzuki reaction with isoquinoline-4-boronic acid took place to give Compound **5**, which deprotected by boron trichloride to yield the target compounds FS23.

B. Protein purification and crystallization

The vector containing the gene of human Hsp90α N-terminal domain (residues 9-236) was cloned into a pET28a vector and the recombinant plasmid was transformed into *E. coli* Rosetta (DE3) pLysS for over-expression (Invitrogen, Carlsbad, USA). The bacteria were grown in 800 mL of LB (Luria-Bertani) broth at 37 °C to an OD_{600} of 0.6–0.8 and then induced by 200 μM IPTG (isopropyl β-D-thiogalactopyranoside) for 3–5 h at 30 °C. The bacteria were collected by centrifugation at 10 000 g for 10 min (CF16RX, Hitachi). The precipitate was re-suspended in buffer A (100 mM Tris/Hcl buffer, pH 7.5, 300 mM NaCl and 5% glycerol) and then crushed by JNBIO 3000 plus (JNBI). The product was centrifuged at 30 000 g for 30 min at 4 °C and the supernatant was loaded onto a 5 mL Ni-NTA (Ni^{2+}-nitrilotriacetate) column (GE Healthcare) and protein was eluted with buffer B (100 mM Tris-Hcl buffer, pH 7.5, 300 mM NaCl, 100 mM imidazole, and 5% glycerol). The protein product was concentrated and buffer-exchanged to buffer C (100 mM Tris-Hcl buffer, pH 7.5, 300 mM NaCl and 5% glycerol) using an Amicon Ultra-15, 10000 Mr cut-off centrifugal concentrator (Millipore). For further purification, the impurities were removed by a Superdex 75 PG gel-filtration column (GE Healthcare) with buffer C. Positive fractions were analysed by a 15% SDS-PAGE to determine the purity. The protein was flash-frozen in liquid nitrogen and stored at −80 °C.

For crystallization, the purified Hsp90 N-terminal domain was concentrated in Amicon Ultra-15, 10 000 Mr cut-off centrifugal concentrator to a concentration of about 20 mg/mL. The small molecule FS23 was added to protein with a 5 : 1 molar ratio and the mixture was incubated for 1 h at 4 °C. After incubation, the mixture was centrifuged for 10 min and the precipitation was removed from the system. The supernate was analysed by DLS (dynamic light scattering, Malvern) to determine whether the complex was suitable for crystallization. This was done following the standard protocols supplied by the manufacturer. Crystallization was carried out at 4 °C using the hanging drop vapor diffusion method and the cocrystals were grown under similar conditions previously described for native crystal [31], with a little difference, 100 mM Tris-HCl, pH 8.5, 20% PEG 4000, 200 mM $MgCl_2$.

C. Data collection, structure determination, and refinement

Crystals were mounted and flash-frozen in liquid nitrogen for diffraction test and data collection. All data sets were collected at 100 K on beamline BL17U1 at Shanghai Synchrotron Radiation Facility (SSRF) [32] and processed with the HKL2000 software package [33]. The structures were solved by molecular replacement, using the PHENIX [34]. The search model used for the crystal was the previously reported structure of the $Hsp90^N$ (PDB code 3T0H) [31], the structures were refined using PHENIX [34]. With the aid of the program Coot [35], water molecules and others were fitted into to the initial Fo-Fc map. The complete statistics, as well as the quality of the solved structure, are shown in Table 1.

TABLE 1. Statistics for data processing and model refinement of human Hsp90^{N}-FS23 complex

Diffraction source	BL17U1, SSRF[a]
Diffraction data	
Resolution (Å)	34.85–1.70 (1.73–1.80)
Space group	I222
Unit cell parameters	
a, b, c (Å)	70.06, 88.27, 97.00
α, β, γ (°)	90.00, 90.00, 90.00
Wavelength (Å)	0.9792
Total reflections	119370
Unique reflections	33536
Redundancy	3.8 (3.7)
I/σ(I)	36.4 (2.7)
Completeness (%)	94.2 (97.7)
R_{merge} (%)	48 (59.2)
Refinement data	
Reflections in working set	33536
Reflections in test set	1733
R_{work} /R_{free} (%)	18.5/21.4
Mean temperature factor (Å^2)	32.7
Bond lengths (Å)	0.006
Bond angles (°)	0.99

[a] Data in parentheses are for the highest-resolution shell.

III. RESULTS AND DISCUSSION

A. Purification of Hsp90^{N}

Hsp90^{N} was purified to apparent homogeneity using metal-chelating column, followed by gel filtration chromatography. The elution volume peak corresponds to monomeric Hsp90^{N} with an apparent molecular weight of 25 kDa and showed a good purity (the purity of protein was assessed by SDS-PAGE to be 98%), as shown in Fig. 2(a). The protein and FS23 were mixed at 1 : 5 molar ratio, and the result of DLS showed that there was only one peak which abided by the Gauss distribution, indicating that the diameter of particles was almost uniform. The PDI (Polydispersity Index) was 13.7%, so it is conceivable that nearly all the complex existed in monomer, as shown in Fig. 2(b). All these data demonstrated that this mixture was suitable for crystallization.

B. Crystallization and structure determination

After 3–4 days, crystals were grown, with an average dimension of approximately 200 µm × 100 µm × 50 µm (Fig. 3). Diffraction data were collected to ∼ 1.70 Å resolution (Fig. 4) and indexed in space groups I222. The unit-cell parameters were a = 70.06 Å, b = 88.27 Å, c = 97.00 Å; $\alpha = 90°$, $\beta = 90°$ and $\gamma = 90°$.

The structure of Hsp90^{N}-FS23 was solved by molecular replacement using the known 3-D structure of Hsp90^{N} as a search model (PDB code 3T0H), determined at 1.70 Å resolution (PDB code 5CF0) [31]. In the crystal structure, FS23 binds to the ATP-binding pocket completely and its intact

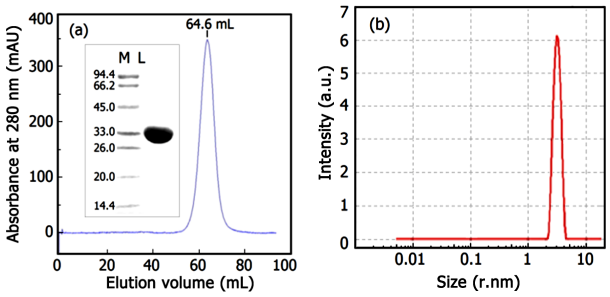

Fig. 2. (Color online) Purification of Hsp90^{N}. (a) Size-exclusion chromatography and SDS-PAGE analysis of purified Hsp90^{N}. The flow rate was 1 mL/min and a single peak was observed for the purified protein solution. Lane M contains molecular weight marker (labeled in kDa). (b) Distribution of DLS. Hsp90^{N} and FS23 were mixed at 1 : 5 molar ratio and the concentration of the protein is 2 mg/mL. There is only one peak in the diagram which shows that the complex is almost monodisperse and would be ideally suited for crystal growth.

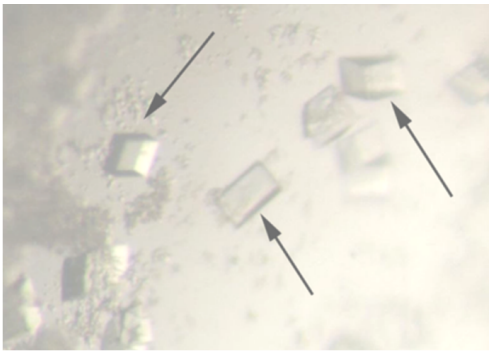

Fig. 3. (Color online) Crystals of the Hsp90^{N}-FS23 complex obtained by the hanging-drop method at 277 K. The average dimensions of the crystals were approximately 200 µm × 100 µm × 50 µm.

electron density has been captured, as shown in Fig. 5(a). So we have reason to believe that FS23 was fully bound into Hsp90^{N} in the complex structure.

The refined model contains residues Val17-Lys224 and no electron density was observed for residues Asp9-Glu16 and Glu225-Glu236 in the structure. The missing residues are at the N- and C-termini of the model and are presumed to be disordered.

C. Analysis of crystal structure of Hsp90^{N}-FS23 complexes

Although the refined structure of Hsp90^{N}-FS23 differs from that of Hsp90^{N} (PDB code 3T0H) in resolution level, no significant conformational changes were observed between the two protein structures, as shown in Fig. 6(a). But there are some tiny differences from Asp102 to Tyr139 in the two structures. The complex structure of Hsp90^{N}-FS23 provides the structural basis to further investigate the activated confor-

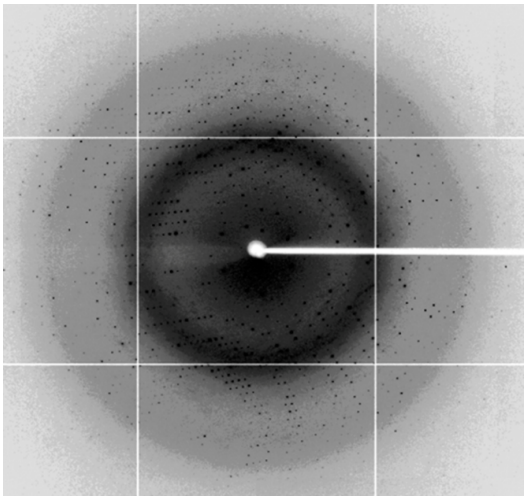

Fig. 4. X-ray diffraction from Hsp90^{N}-FS23 complex crystal. The diffraction pattern was recorded on a ADSC Q315r detector with 0.9792 Å wavelength X-rays on beamline BL17U1 at SSRF, 0.5° oscillation, 0.3 s exposure and 200 mm sample-to-detector distance.

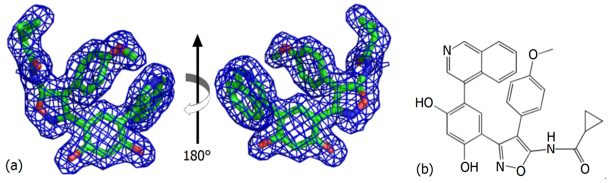

Fig. 5. (Color online) Structure of FS23. (a) Stereo view of the FS23 (2Fo-Fc) electron density before any FS23 atoms were built into the Hsp90 model. The blue mesh, contoured at 1.0σ, is the refined FS23 model in a stick representation. Carbon, nitrogen and oxygen atoms are shown in green, blue and red, respectively. (b) Chemical structure of FS23.

mational change of Hsp90 after FS23 binding. Superimposition of Hsp90^{N}-FS23 complex with the native Hsp90^{N} structures shows that the H4 (amino acids from Thr99) to Leu107 and H5 (amino acids from Gly114 to Ala124) of Hsp90^{N} undergo a conformational rearrangement in response to the bound FS23 (Fig. 6(b)).

The crystal packing patterns of Hsp90^{N}-FS23 (I222) and Hsp90^{N}-ATP (P21) is different, and the Met98 to Tyr139 in the two structures are different, too (Fig. 6(c)). In the complex of Hsp90^{N}-ATP, a loop containing amino acids from Leu107 to Thr115, called L6 (Fig. 6(d)). The ATP lid consisting of H4-L6-H5-H6 secondary structure elements has two different conformations in Hsp90^{N} which is essential for the function of Hsp90 in regulating the entrance and width of the pocket. In free Hsp90^{N} the lid is in open conformation and the pocket is about 12 Å in diameter near its entrance. When the ATP binds to the pocket, H4 and H5 undergo helix-to-coil and coil-to-helix transition which impel L6 moving into the pocket to replace the H4 as one of the pocket walls. Then the ATP lid changes into closed conformation. The functional consequence is that the L6 loop acts as a gate to constrict the pocket entrance from a width of 12 Å to 8 Å [9]. Only when the ATP

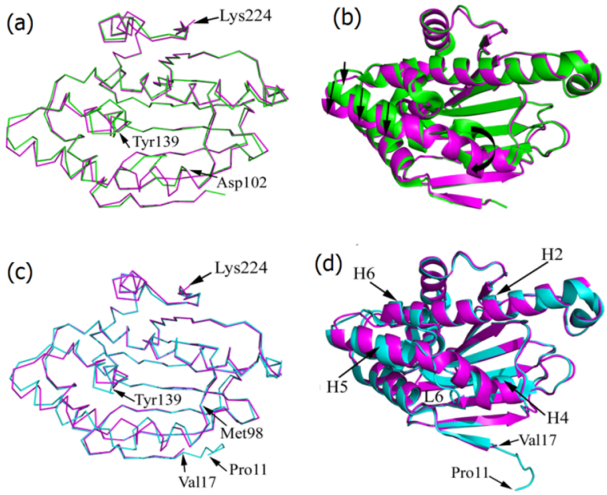

Fig. 6. (Color online) Comparison of crystal structures of Hsp90^{N}-FS23 (magenta) with Hsp90^{N} (green) and Hsp90^{N}-ATP (cyan) complexes: ribbon (a) and cartoon (b) superimpositions of crystal structures of Hsp90^{N}-FS23 and Hsp90^{N}, and ribbon (c) and cartoon (d) superimpositions of crystal structures of Hsp90^{N}-FS23 and Hsp90^{N}-ATP complexes.

lid is in open conformation, Hps90 can interact with its client proteins to accomplish conformational maturation and activation. But there is only a big helix from Thr99 to Ala124 in Hsp90^{N}-FS23, that is the L6 loop was substituted by helix, which means that even though there is substrate bind to Hsp90, conformational change would not happen, resulting in its interaction with client proteins failed (Fig. 6(d)). The disappearance of L6 in complex Hsp90^{N}-FS23 plays an important role in explaining why FS23 could block up the function of Hsp90.

Electrostatic potential surface surrounding the active site of Hsp90N-FS23 and Hsp90N-ATP are shown in Fig. 7. In common with the structure of Hsp90N-ATP, FS23 binding site of Hsp90 is located in the ATP binding site adopts the shape of a cleft (Fig. 7(a)). It is interesting that the binding of inhibitor induce structural rearrangements of L6 and produced a hole in the structure (Fig. 7(a)).

D. Interactions between Hsp90^{N} and FS23

There are two direct hydrogen bonds between Hsp90^{N} and FS23. One is the interaction between FS23 and Asp93, with the distance of 2.7 Å. The other is the interaction between FS23 and Thr184, with the distance of 3.5 Å. A π-π stacking interactions were formed between the side chain of the residue Phe138 and aromatic rings of FS23. FS23 forms water-mediated HBs with residues Leu48, Ser52, Ile96, Asp102 and Gly135. The hydrogen bond network between Hsp90^{N} and FS23 is the most critical portion of the interface and they make FS23 combine Hsp90^{N} effectively (Fig. 8). What's more, there is extensive, though not complete, surface complementarity between FS23 and the pocket, and this

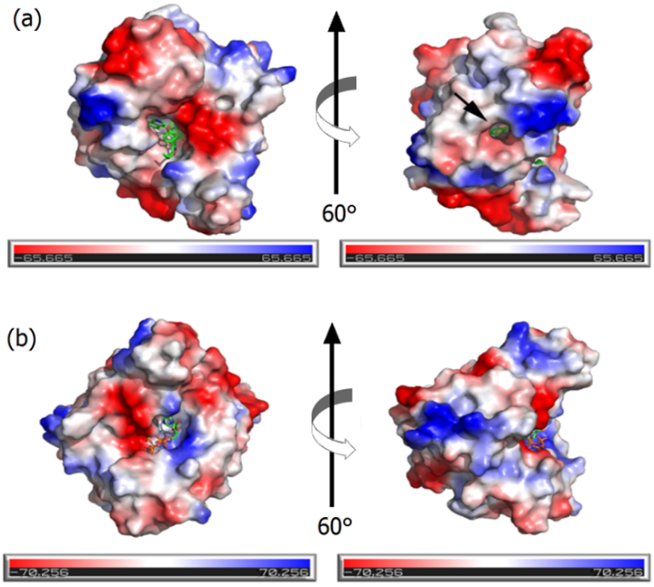

Fig. 7. (Color online) Electrostatic potential surface distribution of Hsp90. (a) Electrostatic potential surface near the FS23-binding site. (b) Electrostatic potential surface near the ATP-binding site. The protein surface is colored to reflect the electrostatic potential, red for negative charge and blue for positive charge, FS23 and ATP in stick representation.

allows for a high density of van der Waals contacts.

Superimposition of Hsp90^{N}-FS23 (PDB code 5CF0) with Hsp90^{N}-ATP (PDB code 3T0Z) and Hsp90^{N}-GDM (PDB code 1YET) structures revealed that the FS23, ATP and GDM occupied the same location, with some subtle difference in the chemical group, though. In the complex of Hsp90^{N}-GDM (PDB code 1YET) for example, geldanamycin nearly occupies the whole pocket and there is no much room for modification. So it is hard to see significant changes in solubility, bioavailability and hepatotoxicity in derivatives of geldanamycin. But the situation is different for FS23 binding and there is enough room for redesigning and reform of FS23 to obtain derivatives with better qualities (Fig. 9).

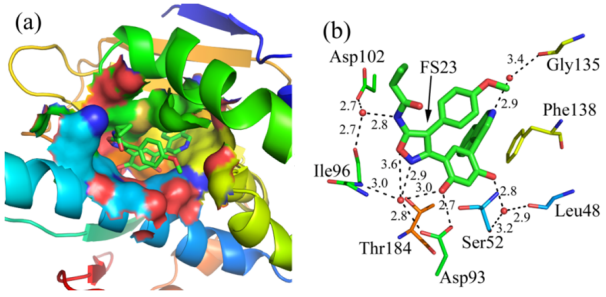

Fig. 8. (Color online) Interactions between Hsp90^{N} and FS23. (a) Surface representation of FS23 bound in the pocket of Hsp90^{N}, protein and FS23 present in cartoon and stick, respectively. (b) Interactions between Hsp90^{N} and FS23. Hydrogen bonds are shown by black dashed lines with distances between two atoms labeled. Water molecules are shown as red spheres.

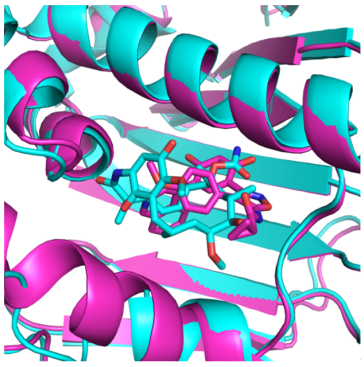

Fig. 9. (Color online) Comparison of the crystal structures of Hsp90^{N}-FS23 with Hsp90^{N}-GDM complexes. Superimposition of Hsp90^{N}-FS23 (magenta, PDB code 5CF0) and Hsp90^{N}-GDM (cyan, PDB code 1YET).

The pocket is mostly polar at its entrance, so hydrophilic groups which can interact with polar amino acids could be added to FS23 to increase the solubility of small molecule. While it becomes predominantly hydrophobic near the pocket bottom, derivatives with increased affinity for Hsp90 may be yielded if groups with non-hydrogen atoms are added to FS23 and hydrogen bond complementarity is increased. The most interesting portion of the interface in the complex Hsp90^{N}-FS23 is the hole produced by structural rearrangements of L6. There is neither a direct nor an indirect interaction between residues in the hole and FS23. So groups can be added to FS23 to fill the cavity and interact with residues in the hole to increase the activity of derivatives.

IV. CONCLUSION

The structure of Hsp90^{N} reveals a pronounced pocket which is highly conserved. And residues in the pocket are confirmed essential in keeping the protein activity. Compound FS23 is designed to interact with these residues in the pocket and has been certified as a potential inhibitor for Hsp90. In the crystal structure, intact electron density of FS23 has been captured, and we have reason to believe that FS23 was fully bound into Hsp90^{N} in the complex structure.

There are some differences from Met98 to Tyr139 in the two structures of Hsp90^{N}-FS23 and Hsp90^{N}-ATP. The disappearance of L6 in complex Hsp90^{N}-FS23 plays an important role in explaining why FS23 could block up the function of Hsp90. And it is interesting that the binding of inhibitor induce structural rearrangements of L6 and produced a hole in the structure.

Superimposition of Hsp90^{N}-FS23 with Hsp90^{N}-GDM structures revealed that the FS23 and GDM occupied the same location but some subtle different in the chemical group. And there is enough room for redesigning and reform of FS23 to obtain derivatives with better qualities. Hydrophilic groups which can interact with polar amino acids could be added to FS23 to increase the solubility of small molecule and groups could be added to FS23 to fill the cavity which produced by structural rearrangements of L6 and interact with residues

in the hole to increase the activity of derivatives. Generally speaking, there is much room for FS23 to get derivatives with great characters and the pattern of FS23 binding to $Hsp90^N$ provides us a new idea to design inhibitors for proteins.

This new Hsp90 inhibitor FS23 directs a territory by extending the ligands to a less explored sub-pocket and provides a potential chemotype for Hsp90 inhibitor development. The structure of $Hsp90^N$-FS23 offers details of protein-inhibitor interactions and holds the promise of novel, more effective, safer and cheaper drugs.

Each year, new targets are being identified, structures of those targets are being determined at an amazing rate, and our capability to capture a quantitative picture of the interactions between targets and ligands is accelerating. SBDD is a powerful method, especially when used as a tool within an armamentarium for discovering new drug leads against important targets. After a target and a structure of that target are chosen, new leads can be designed from chemical principles and can create a very promising lead which can continue to Phase I clinical trial.

[1] Scapin G. Structural biology and drug discovery. Curr Pharm Design, 2006, **12**: 2087–2897. DOI: 10.2174/138161206777585201

[2] Ennifar E. X-ray crystallography as a tool for mechanism-of-action studies and drug discovery. Curr Pharm Biotechno, 2013, **14**: 537–550. DOI: 10.2174/1389201014051311111104824

[3] Prodromou C, Roe S M, O'Brien R, *et al*. Identification and structural characterization of the ATP/ADP-binding site in the Hsp90 molecular chaperone. Cell, 1997, **90**: 65–75. DOI: 10.1016/S0092-8674(00)80314-1

[4] Sato T, Minagawa S, Kojima E, *et al*. HtpG, the prokaryotic homologue of Hsp90, stabilizes a phycobilisome protein in the cyanobacterium *Synechococcus elongatus* PCC 7942. Mol Microbiol, 2010, **76**: 576–589. DOI: 10.1111/j.1365-2958.2010.07139.x

[5] Harris S F, Shiau A K and Agard D A. The crystal structure of the carboxy-terminal dimerization domain of htpG, the Escherichia coli Hsp90, reveals a potential substrate binding site. Structure, 2004, **12**: 1087–1097. DOI: 10.1016/j.str.2004.03.020

[6] Stebbins C E, Russo A A, Schneider C, *et al*. Crystal structure of an Hsp90–geldanamycin complex: targeting of a protein chaperone by an antitumor agent. Cell, 1997, **89**: 239–250. DOI: 10.1016/S0092-8674(00)80203-2

[7] Caplan A J. Hsp90's secrets unfold: new insights from structural and functional studies. Trends Cell Biol, 1999, **9**: 262–268. DOI: 10.1016/S0962-8924(99)01580-9

[8] Pratt W B and Toft D O. Regulation of signaling protein function and trafficking by the hsp90/hsp70-based chaperone machinery. Exp Biol Med, 2003, **228**: 111–133. DOI: 10.1002/9781118063903.ch6

[9] Picard D. Heat-shock protein 90, a chaperone for folding and regulation. Cell Mol Life Sci, 2002, **59**: 1640–1648. DOI: 10.1007/PL00012491

[10] Maloney A and Workman P. Hsp90 as a new therapeutic target for cancer therapy: the story unfolds. Expert Opin Biol Th, 2002, **2**: 3–24. DOI: 10.1517/14712598.2.1.3

[11] Kamal A, Thao L, Sensintaffar J, *et al*. A high-affinity conformation of Hsp90 confers tumour selectivity on Hsp90 inhibitors. Nature, 2003, **425**: 407–410. DOI:10.1038/nature01913

[12] Chiosis G, Lucas B, Shtil A, *et al*. Development of a purine-scaffold novel class of Hsp90 binders that inhibit the proliferation of cancer cells and induce the degradation of Her2 tyrosine kinase. Bioorgan Med Chem, 2002, **10**: 3555–3564. DOI:10.1016/S0968-0896(02)00253-5

[13] Supko J G, Hickman R L, Grever M R, *et al*. Preclinical pharmacologic evaluation of geldanamycin as an antitumor agent. Cancer Chemoth Pharm, 1995, **36**: 305–315. DOI: 10.1007/BF00689048

[14] Roe S M, Prodromou C, O'Brien R, *et al*. Structural Basis for Inhibition of the Hsp90 Molecular Chaperone by the Antitumor Antibiotics Radicicol and Geldanamycin. J Med Chem, 1999, **42**: 260–266. DOI: 10.1021/jm980403y

[15] Pearl L H and Prodromou C. Structure and mechanism of the Hsp90 molecular chaperone machinery. Annu Rev Biochem, 2006, 75: 271–294. DOI: 10.1146/annurev.biochem.75.103004.142738

[16] Shiau A K, Harris S F, Southworth D R, *et al*. Structural analysis of E. coli hsp90 reveals dramatic nucleotide-dependent conformational rearrangements. Cell, 2006, **127**: 329–340. DOI: 10.1016/j.cell.2006.09.027

[17] Wandinger S K, Richter K and Buchner J. The Hsp90 chaperone machinery. J Biol Chem, 2008, **283**: 18473–18477. DOI: 10.1074/jbc.R800007200

[18] Al Shaer L, Walsby E, Gilkes A, *et al*. Heat shock protein 90 inhibition is cytotoxic to primary AML cells expressing mutant FLT3 and results in altered downstream signaling. Brit J Haematol, 2008, **141**:483–93. DOI: 10.1111/j.1365–2141.2008.07053.x

[19] Jilani K, Qadri S and Lang F. Geldanamycin-induced phosphatidylserine translocation in the erythrocyte membrane. Cell Physiol Biochem, 2013, **32**: 1600–1609. DOI: 10.1159/000356596

[20] Li Y Y, Zhang T and Sun D X. New developments in Hsp90 inhibitors as anti-cancer therapeutics: mechanisms, clinical perspective and more potential. Drug Resist Update, 2009, **12**: 17–27. DOI: 10.1016/j.drup.2008.12.002

[21] Egorin M J, Lagattuta T F, Hamburger D R, *et al*. Pharmacokinetics, tissue distribution, and metabolism of 17-(dimethylaminoethylamino)-17-demethoxygeldanamycin (NSC 707545) in CD 2 F 1 mice and Fischer 344 rats. Cancer Chemoth Pharm, 2002, **49**: 7–19. DOI: 10.1007/s12272-010-1213-2

[22] Schulte T W and Neckers L M. The benzoquinone ansamycin 17-allylamino-7-demethoxygeldanamycin binds to HSP90 and shares important biologic activities with geldanamycin. Cancer Chemoth Pharm, 1998, **42**: 273–279. DOI: 10.1007/s002800050817

[23] Sydor J R, Normant E, Pien C S, *et al*. Development of 17-allylamino-17-demethoxygeldanamycin hydroquinone hydrochloride (IPI-504), an anti-cancer agent directed against Hsp90. P Natl Acad Sci USA, 2006, **103**: 17408–17413. DOI: 10.1073/pnas.0608372103

[24] Zhang T, Hamza A, Cao X H, *et al*. A novel Hsp90 inhibitor to

disrupt Hsp90/Cdc37 complex against pancreatic cancer cells. Mol Cancer Ther, 2008, **7**: 162–170. DOI: 10.1158/1535-7163.MCT-07-0484

[25] Porter J R, Fritz C C and Depew K M. Discovery and development of Hsp90 inhibitors: a promising pathway for cancer therapy. Curr Opin Chem Biol, 2010, **14**: 412–420. DOI: 10.1016/j.cbpa.2010.03.019

[26] Neckers L. Development of small molecule Hsp90 inhibitors: Utilizing both forward and reverse chemical genomics for drug identification. Curr Med Chem, 2003, **10**: 733–739. DOI: 10.2174/0929867033457818#sthash.6kGY1Nyp.dpuf

[27] Murray C W, Verdonkv M L and Rees D C. Experiences in fragment-based drug discovery. Trends Pharmacol Sci, 2010, **33**: 224–232. DOI: 10.1016/j.tips.2012.02.006

[28] Chen D, Shen A, Li J, *et al*. Discovery of potent N-(isoxazol-5-yl)amides as HSP90 inhibitors. Eur J Med Chem, 2014, **87**: 765–781. DOI: 10.1016/j.ejmech.2014.09.065

[29] Ren J, Li J, Wang Y, *et al*. Identification of a New Series of Potent Diphenol HSP90 Inhibitors by Fragment Merging and Structure-based Optimization. Bioorg Med Chem Lett, 2014, **24**: 2525–2529. DOI: 10.1016/j.bmcl.2014.03.100

[30] Ren J, Yang M, Liu H, *et al*. Multi-substituted 8-aminoimidazo[1,2-a]pyrazines by Groebke-Blackburn-Bienaymé reaction and their Hsp90 inhibitory activity. Org Biomol Chem, 2015, **13**:1531–5. DOI: 10.1039/c4ob01865f

[31] Li J, Sun L, Xu C, *et al*. Structure insights into mechanisms of ATP hydrolysis and the activation of human heat-shock protein 90. Acta Biochim Biophys Sin, 2012, **44**: 300–306. DOI: 10.1093/abbs/gms001

[32] Wang Q S, Yu F, Huang S, *et al*. The macromolecular crystallography beamline of SSRF. Nucl Sci Tech, 2015, **26**: 010102. DOI: 10.13538/j.1001–8042/nst.26.010102

[33] Otwinowski Z and Minor W. Processing of X-ray diffraction data collected in oscillation mode. Method Enzymol, 1997, **276**: 307–326. DOI: 10.1016/S0076-6879(97)76066-X

[34] Adams P D, Afonine P V, Bunkoczi G, *et al*. PHENIX: a comprehensive Python-based system for macromolecular structure solution. Acta Crystallogr D, 2010, **66**: 213–221. DOI: 10.1107/S0907444909052925

[35] Emsley P and Cowtan K. Coot: Model-building tools for molecular graphics. Acta Crystallogr D, 2004, **60**: 2126–2132. DOI: 10.1107/S0907444904019158